Electromagnetic Compatibility Analysis of an Induction Motor Drive With Integrated Power Converter

Tianyu Chen[1], Carlos Caicedo-Narvaez[1], Haokun Wang[1], Mehdi Moallem[2], Babak Fahimi[1], and Morgan Kiani[3]

[1]Electrical and Computer Engineering Department, The University of Texas at Dallas, Richardson, TX 75080 USA
[2]Electrical and Computer Engineering Department, Isfahan University of Technology, Isfahan 841583111, Iran
[3]Department of Engineering, Texas Christian University, Fort Worth, TX 76129 USA

With the development of high-temperature wide bandgap power semiconductors, such as SiC MOSFET and GaN HEMT, it becomes possible to integrate the power converter directly into motors. However, the leakage magnetic flux in the motor may cause interference with the operation of the electronic circuit. In this article, the electromagnetic compatibility of the power converter integrated in an induction motor is investigated. The simulation shows that the leakage magnetic flux of the end-winding will penetrate into the nearby area, and it will cause interference with the Hall-effect current sensors if the power converter is mounted in the space between the motor end cap and the end-winding. A prototype of the GaN-HEMT-based power converter is built and integrated into a 3-hp induction motor. The leakage magnetic flux is scanned by the linear Hall-effect sensors and the measured result is aligned with the finite-element simulation.

***Index Terms*—Electromagnetic compatibility, induction motor, integrated motor drive system, power converter integration.**

I. Introduction

BENEFITTING from the higher junction temperature and faster switching speed of wide bandgap power semiconductors [1]–[3], the power density of high-frequency power converters has been significantly increased [4], [5]. A typical variable frequency drive system with an external SiC-MOSFET-based converter is shown in Fig. 1. The high dv/dt on the long power cable (i.e., the dv/dt of SiC MOSFET is up to 15 kV/μs) can cause severe overvoltage problem on the motor winding [6]. The overvoltage problem can potentially damage the insulation and significantly shorten the lifetime of a motor. To mitigate the dv/dt problem and decrease the size of the whole system, one of the solutions is to integrate the power converter directly into the motor.

The state-of-the-art technologies of power electronics integrated into motor drives are summarized in [7] and [8]. One of the methods is to integrate the power converter into the terminal box at the cost of increasing the motor size. Another technology is based on mounting the power converter in the space between the end cap and the end-winding and using a metal barrier to shield the magnetic flux and the heat generated by the motor winding. Although the electromagnetic compatibility and thermal problems are addressed, the stack length is extended.

To avoid the drawbacks of the existing technologies, an integrated motor drive system without increasing the original size and stack length is introduced and investigated. The model of the integrated motor drive system is shown in Fig. 2. Compared with previous studies, the proposed integrated motor drive system works in a more exposed environment with stronger magnetic field and higher temperature. As the power converter is directly exposed to the end-winding, the leakage magnetic field from the end-winding will couple with the components of the power converter. To validate the feasibility of the integrated power converter operating in such an environment, the impacts of the leakage magnetic field on the fundamental frequency are investigated through ANSYS Electronics Desktop.The simulation results show that the leakage magnetic-flux density decays significantly with the increasing distance from the end-winding; however, the Hall-effect current sensors of the power converter will still be impacted by the leakage magnetic field. To validate the finite-element simulation results, a GaN-HEMT-based power converter is built and integrated into a 3-hp induction motor. The leakage magnetic flux on the surface of the printed-circuit board (PCB) is scanned by the linear Hall-effect sensors.

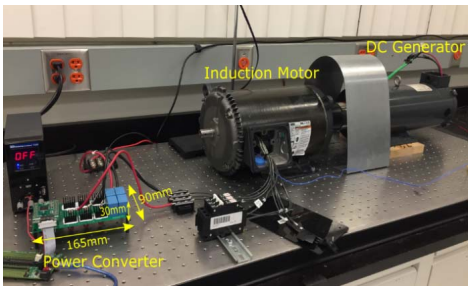

Fig. 1. Typical variable frequency drive system.

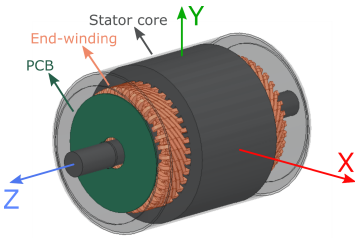

Fig. 2. 3-D model of the 3-hp induction motor with PCB mounted.

Manuscript received July 20, 2019; revised September 25, 2019; accepted October 22, 2019. Date of current version December 20, 2019. Corresponding author: T. Chen (e-mail: tianyu.chen1@utdallas.edu).

Color versions of one or more of the figures in this article are available online at http://ieeexplore.ieee.org.

Digital Object Identifier 10.1109/TMAG.2019.2949518

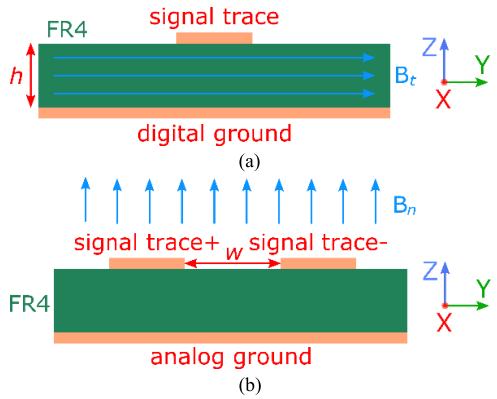

Fig. 3. Cross section of the PCB layout. (a) Single-ended trace is impacted by the external magnetic field in the tangential direction. (b) Differential trace is impacted by the external magnetic field in the normal direction.

The remainder of this article is organized as follows. Section II analyzes the interaction between the external magnetic field and the components of the power converter. The modeling and the finite-element simulation of a 3-hp integrated motor drive system are implemented in Section III. The leakage magnetic flux on the surface of the PCB is experimentally measured by the linear Hall-effect sensors and compared with the simulated results, which are described in Section IV. Finally, Section V summarizes the conclusions and identifies the direction for future work.

II. Electromagnetic Compatibility of Electronic Circuit Under External Magnetic Field

Power electronics converters comprise the microcontroller, power semiconductor switches, gate drivers, current sensors, auxiliary voltage regulators, and the traces for connections of analog signals and digital signals. To ensure the proper operation of the power converter under the external magnetic field, the electromagnetic compatibility of these components is analyzed.

A. Interaction Between External Magnetic Field and Traces

On the layout of a PCB, the connections of digital signals are routed by single-ended traces and the connections of analog signals are routed by differential traces as shown in Fig. 3.

As the single-ended trace is sensitive to the tangential magnetic field and the differential trace is sensitive to the normal magnetic field, the noise on the traces is given as follows:

$$\begin{cases} v_{\text{noise\_}s} = lh\omega B_t \\ v_{\text{noise\_}d} = lw\omega B_n \end{cases} \tag{1}$$

where l is the length of the trace and ω is the frequency of the magnetic field. The tangential magnetic field is defined as the magnetic field parallel to the PCB surface and the normal magnetic field is defined as the magnetic field perpendicular to the PCB surface. As the direction of traces is arbitrary, the maximum tangential magnetic field is calculated as follows:

$$\begin{cases} B_{t\_\max} = \sqrt{B_x^2 + B_y^2} \\ B_n = B_z. \end{cases} \tag{2}$$

To ensure the integrity of signals, such as the pulsewidth modulation (PWM) signals, the noise on the trace must be a tolerable value, and thus, the maximum magnetic field can be calculated.

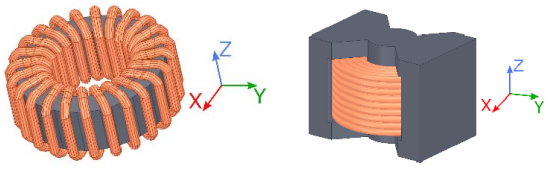

Fig. 4. Magnetic components. (a) Toroidal-type magnetic core. (b) PQ-type magnetic core.

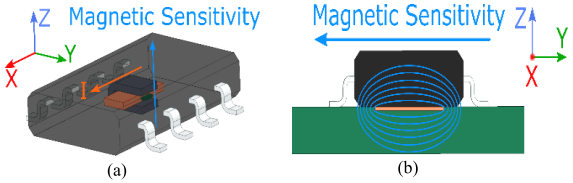

Fig. 5. Surface-mounted Hall-effect current sensor. (a) Internal current-type sensor. (b) External current-type sensor.

B. Interaction Between External Magnetic Field and Magnetic Components

The magnetic components in a power converter are used for the auxiliary voltage regulator and the isolated power supply of the floating gate driver. The toroidal core and PQ-core-based magnetic components are shown in Fig. 4. As the magnetic field of the toroidal core is totally surrounded by the coil, the toroidal core has very high immunity to the external magnetic field. However, the PQ-core-based magnetic components will capture extra voltage under the external magnetic field. The noise of the PQ core magnetic components caused by the external magnetic field is given as follows:

$$v_{\text{noise\_}PQ} = NA_c\omega B_n \tag{3}$$

where N is the number of turns and A_c is the average cross-sectional area of the coil. To ensure the proper function of the magnetic components, the noise voltage must be sufficiently low.

C. Interaction Between External Magnetic Field and Hall-Effect Current Sensor

Due to the limited space of the integrated power converter, the surface-mounted current sensors must be used to obtain the minimum vertical size. Two types of surface-mounted Hall-effect current sensors are shown in Fig. 5. Both of these sensors use the open-loop measurement [9], that is, to measure the current amplitude from its resulting magnetic field. According to this principle, the Hall-effect current sensor is very sensitive to the external magnetic field [10]. The internal current-type sensor uses a U-shaped ferrite core to strengthen the magnetic field, and it is sensitive to the external magnetic field in the normal direction. Whereas for the external current-type sensor, the current goes through the trace underneath the sensor, and the sensor measures the magnetic field directly. In this case, the external current-type sensor is sensitive to the external magnetic field in the tangential direction.

The impact of the external magnetic field on the critical electronic components of a power converter is analyzed in this section. To ensure the proper operation of these components, the maximum permissible external magnetic field can be calculated with the typical dimensions and parameters of the components. The results are given in Table I. It should be noted that as the analog signal is more sensitive to the noise

TABLE I
MAXIMUM PERMISSIBLE EXTERNAL MAGNETIC FIELD

Components	B_n	B_t
Trace	10mT	200mT
Magnetic components	25mT	--
Hall-effect current sensor	0.5mT	0.1mT

TABLE II
PARAMETERS OF THE INDUCTION MOTOR

Parameter	Dimension
Stator Length	130mm
Stator Outer Diameter	200mm
Stator Inner Diameter	120mm
Air Gap	0.35mm
Pole Pairs	2
Stator Slots	36
Rotor Slots	8
Turns per Coil	17

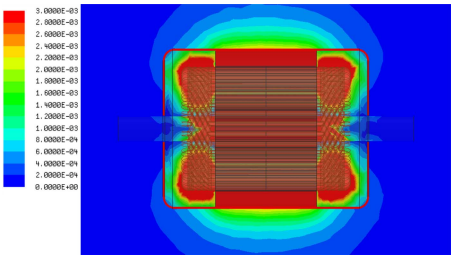

Fig. 6. Leakage magnetic field caused by the end-winding.

than the digital signal, the single-ended trace can sustain higher external magnetic field than the differential trace. If the external magnetic field is lower than the maximum permissible value, the operation of the power converter is ensured. Otherwise, the replacement solution or magnetic shielding must be implemented.

III. MODELING AND SIMULATION OF THE INTEGRATED MOTOR DRIVE SYSTEM

To investigate the impact of the leakage magnetic field on the integrated power converter, a 3-D model of the induction motor is built. The parameters of the 3-hp induction motor are given in Table II.

The rotor is squirrel-cage type with eight aluminum bars. The stator winding is lap type with coil pitch of eight. The power converter is mounted in the space between the end cap and the end-winding. To find the optimal distance from the power converter to the end-winding, this distance is swept from 5 to 20 mm with steps of 5 mm. At every position, the finite-element simulation is performed and the magnetic field on the surface of the PCB is observed.

At the rated power, the magnitude of phase current is 12 A. With sinusoidal current excitation, the simulated magnetic-flux density at the cross section along with the motor axis is shown in Fig. 6. One can notice that most of the magnetic flux is concentrated in the magnetic core. The magnitude of the leakage flux density is only a few milli-Tesla.

The magnetic-flux density in the normal direction acting on the surface of the PCB with clearance to the end-winding is swept from 5 to 20 mm. With simulation convergence criterion of 0.1%, the snapshots of the magnetic-field distribution are

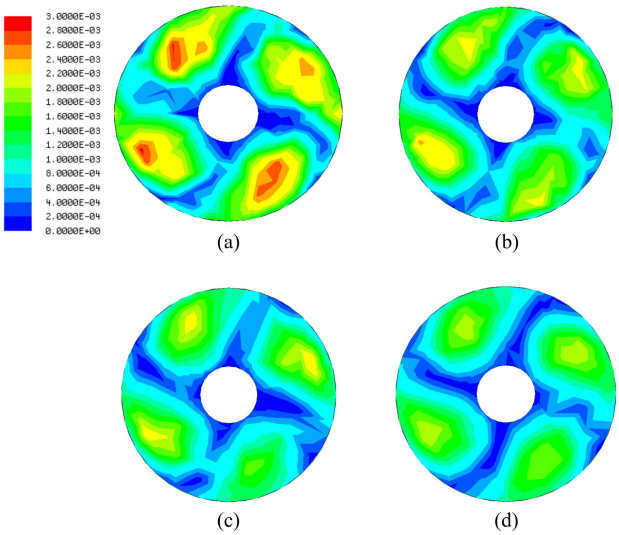

Fig. 7. Magnetic field in the normal direction. (a) 5 mm clearance. (b) 10 mm clearance. (c) 15 mm clearance. (d) 20 mm clearance.

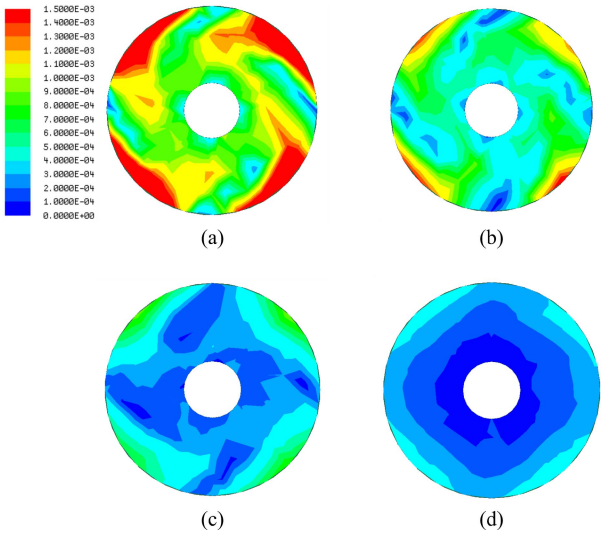

Fig. 8. Magnetic field in the tangential direction. (a) 5 mm clearance. (b) 10 mm clearance. (c) 15 mm clearance. (d) 20 mm clearance.

shown in Fig. 7. According to the results, the maximum magnetic-flux density decreases from 3.0 to 2.0 mT when the clearance increases from 5 to 20 mm. As the leakage magnetic field is much weaker in magnitude than the air-gap magnetic field, the resolution makes the leakage magnetic field appear coarse. The magnetic-flux density in the tangential direction acting on the surface of the PCB with clearance to the end-winding is swept from 5 to 20 mm and the resulting snapshots are shown in Fig. 8. According to the simulation results, the maximum magnetic-flux density decreases from 1.5 to 0.4 mT when the clearance increases from 5 to 20 mm.

Combining the simulation results with the electromagnetic-compatibility analysis in Section II, the optimal distance from the PCB to the end-winding is between 10 and 15 mm, so that the clearance to both end-winding and end cap is sufficient. A comparison of the requirement of the external magnetic field given in Table I reveals that the traces and magnetic components can properly operate under the influence of the leakage magnetic field. However, both the internal current-type and external current-type Hall-effect current sensors will be impacted by the leakage magnetic field, and thus the Hall-effect current sensors cannot be used for the current

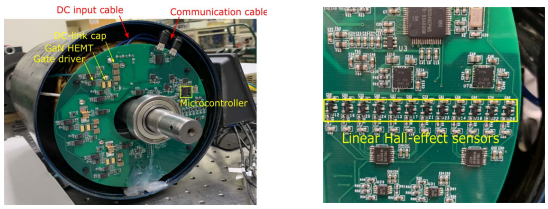

Fig. 9. Integrated motor drive system with the magnetic field detection. (a) GaN-HEMT-based converter. (b) Magnetic field detection.

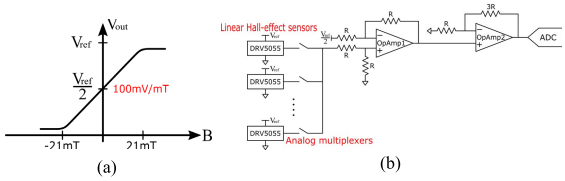

Fig. 10. (a) Characteristics of the linear Hall-effect sensor. (b) Magnetic-field detection circuit.

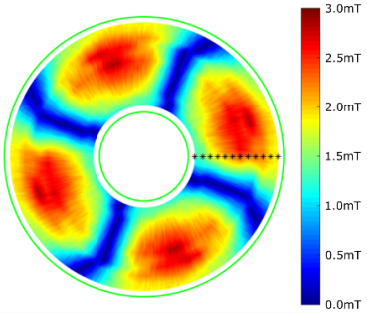

Fig. 11. Measured normal direction magnetic field on the surface of the PCB. The outline of the PCB and the position of linear Hall-effect sensors are marked.

measurement in this integrated motor drive system. As an alternative solution, the shunt resistors can be used, at the cost of higher power loss on the resistance.

IV. Experimental Setup and Validation

Based on the electromagnetic-compatibility analysis and finite-element simulations, a prototype of an integrated motor drive system is built, which is shown in Fig. 9(a). The GaN-HEMT-based power converter is mounted between the end-winding and the end cap with a clearance to the end-winding of 15 mm. Four plastic pillars are inserted between the PCB and the end-winding to make sure the clearance is accurate. Twelve linear Hall-effect sensors are implemented in a row to scan the rotating magnetic field as shown in Fig. 9(b). With the measured magnetic-field distribution on the surface of the PCB, the finite-element simulation results can be validated.

As the normal direction field is much stronger than the tangential direction field, only the normal direction field is experimentally measured to validate the simulation results. Because the leakage magnetic field on the surface of the PCB is only a few milli-Tesla, the low noise linear Hall-effect sensor DRV5055 is used; at the same time, a high-accuracy magnetic-field detection circuit is designed to obtain the optimal resolution [11]. The characteristic of the linear Hall-effect sensor and the magnetic-field detection circuit is shown in Fig. 10. With the help of this design, the accuracy of the magnetic-field measurement is ± 0.05 mT.

The magnetic detection circuit scans the magnetic field every 2° (electrical angle), that is, every degree in spatial angle. The measured normal direction magnetic field is shown in Fig. 11. The measured result portrays a similar pattern and amplitude with the simulation result. However, the maximum magnetic-flux density of the measured result is 2.8 mT, which is higher than 2.4 mT in the simulation result.

V. Conclusion

To integrate the power converter into the motor, the electromagnetic compatibility of electronic components under the low-frequency external magnetic field is investigated. According to the finite-element simulations, the leakage magnetic-flux density caused by the motor end-winding decays with the increasing distance to the end-winding. A proper distance can be selected, so that the impact of leakage magnetic flux can be minimized. As the Hall-effect current sensor is very sensitive to the external magnetic field, a shunt current resistor must be used to measure the current. A prototype of the GaN-HEMT-based power converter is built and integrated into an induction motor. The linear Hall-effect sensors are mounted on the power converter to scan the normal direction magnetic field on the surface of the PCB. The measured results mostly align with those from simulation, which ensures the safe operation of the electronic circuit under the leakage magnetic field.

However, as the wide bandgap power semiconductor device can operate at very high switching frequency and the switching transient is much faster than conventional silicon device, the impact of the high-frequency magnetic field and *dv*/*dt* on the windings must be investigated. At such a high frequency, the traces may act as an antenna at a certain frequency range and the magnetic coupling between the motor winding and the components on the power converter may occur. This research should be addressed in the future work.

References

[1] J. Millán, P. Godignon, X. Perpiñà, A. Pérez-Tomás, and J. Rebollo, "A survey of wide bandgap power semiconductor devices," *IEEE Trans. Power Electron.*, vol. 29, no. 5, pp. 2155–2163, May 2014.

[2] E. A. Jones, F. F. Wang, and D. Costinett, "Review of commercial GaN power devices and GaN-based converter design challenges," *IEEE Trans. Emerg. Sel. Topics Power Electron.*, vol. 4, no. 3, pp. 707–719, Sep. 2016.

[3] T. Funaki *et al.*, "Power conversion with SiC devices at extremely high ambient temperatures," *IEEE Trans. Power Electron.*, vol. 22, no. 4, pp. 1321–1329, Jul. 2007.

[4] J. D. van Wyk and F. C. Lee, "On a future for power electronics," *IEEE Trans. Emerg. Sel. Topics Power Electron.*, vol. 1, no. 2, pp. 59–72, Jun. 2013.

[5] T. Chen, S. Li, and B. Fahimi, "Analysis of DC-link voltage ripple in voltage source inverters without electrolytic capacitor," in *Proc. 44th Annu. Conf. IEEE Ind. Electron. Soc. (IECON)*, Oct. 2018, pp. 1041–1048.

[6] J. He, H. Chen, R. Katebi, N. Weise, and N. A. O. Demerdash, "Mitigation of uneven surge voltage stress on stator windings of induction motors fed by SiC-MOSFET-based adjustable speed drives," in *Proc. IEEE Int. Elect. Mach. Drives Conf. (IEMDC)*, May 2017, pp. 1–7.

[7] T. M. Jahns and H. Dai, "The past, present, and future of power electronics integration technology in motor drives," *CPSS Trans. Power Electron. Appl.*, vol. 2, no. 3, pp. 197–216, Sep. 2017.

[8] W. Lee, S. Li, D. Han, B. Sarlioglu, T. A. Minav, and M. Pietola, "A review of integrated motor drive and wide-bandgap power electronics for high-performance electro-hydrostatic actuators," *IEEE Trans. Transport. Electrific.*, vol. 4, no. 3, pp. 684–693, Sep. 2018.

[9] S. Ziegler, R. C. Woodward, H. H.-C. Iu, and L. J. Borle, "Current sensing techniques: A review," *IEEE Sensors J.*, vol. 9, no. 4, pp. 354–376, Apr. 2009.

[10] *ACS723 High Accuracy, Galvanically Isolated Current Sensor IC With Small Footprint SOIC8 Package*, Allegro MicroSyst., Manchester, NH, USA, Apr. 2015.

[11] *DRV5055 Ratiometric Linear Hall Effect Sensor*, Texas Instrum., Dallas, TX, USA, Jan. 2018.